Fabrication and Characterization of Novel 3D Porous Titanium-6Al-4V Scaffold for Orthopedic Application Using Selective Laser Melting Technique

Attaeyan, Ali; Shahgholi, Mohamad*+

Department of Mechanical Engineering, Najafabad Branch, Islamic Azad University, Najafabad, I.R. IRAN

Khandan, Amirsalar

Department of Mechanical Engineering, Khomeinishahr Branch, Islamic Azad University, Khomeinishahr, I.R. IRAN

ABSTRACT: *The use of metallic 3D printers in medical manufacturing has enabled the creation of complex medical products customized to each patient's specific anatomical information through CAD/CAM. This technology has allowed the examination of three-dimensional (3D) bone scaffolds as models for human bone geometry. Gradually, 3D printing has become a promising tool for creating grafts and scaffolds for bone tissue engineering, particularly in orthopedic fractures. The present study explores the use of a medical-grade titanium alloy coated with chitosan containing wollastonite nanoparticles (WS-NPs) at varying concentrations (0, 5, 10, and 15 wt%) to fabricate a 3D porous metallic scaffold using Selective Laser Melting (SLM). Materials characterization was performed using Scanning Electron Microscopy (SEM) and X-Ray Diffraction (XRD) analysis, while mechanical tests were conducted to determine the compressive strength, fracture toughness, elastic modulus, and Poisson ratio of the samples. The study involved fabricating a 3D porous metallic scaffold using SLM and a medical-grade titanium alloy coated with chitosan containing wollastonite nanoparticles (WS-NPs) at varying concentrations (0, 5, 10, and 15 wt%). The samples were characterized using SEM and XRD analysis, and mechanical tests were conducted to determine their properties. The samples were also subjected to a Simulated Body Fluid (SBF) and phosphate-buffered saline (PBS) test to evaluate their bioactivity and biodegradation rate, as well as an MTT toxicity test. The feasibility of the prostheses was tested for 1, 3, 7, and 14 days, and the results were analyzed. The SEM images and XRD analysis showed the surfaces of scaffold parts produced in nanometer dimensions, confirming the corresponding coating as well as the phases in the scaffold. The sample containing 10 wt% WS-NPs had the highest elastic modulus of about 420 MPa and compressive strength with a coating containing 10 wt% WS-NPs in a chitosan matrix. The results showed that the percentage of porosity changed from 52% to 48% in sample 2 and sample 3, respectively, as the compressive strength increased. The third sample exhibited promising biological behavior for orthopedic applications. The objective of this work is to fabricate and characterize a 3D porous metallic scaffold coated with chitosan*

* *To whom correspondence should be addressed.*
+ *E-mail: m.shahgholi@pmc.iaun.ac.ir*
1021-9986/2024/1/66-82 17/$/6.07

containing wollastonite nanoparticles for bone tissue engineering applications. The study successfully fabricated a 3D porous metallic scaffold using SLM and a medical-grade titanium alloy-coated with chitosan containing wollastonite nanoparticles (WS-NPs) at varying concentrations. The results demonstrated that the sample containing 10 wt% WS-NPs had the highest elastic modulus and compressive strength. The third sample exhibited potential for orthopedic applications due to its promising biological behavior.

KEYWORDS: *Metal 3D printing, Freeze drying, Wollastonite, Bio-nanocomposite, Mechanical properties.*

INTRODUCTION

The use of 3D metal implants has enabled the possibility of creating complex medical products based on the specific anatomical information of each patient through computer-aided design. This advancement allows for the production of customized medical implants tailored to individual patients' specific anatomical needs [1-2]. These implants include three-dimensional (3D) bone scaffolds that can be used for bone tissue engineering, diagnostic systems, and drug delivery to target tissues [2]. *Park et al.* [3] created porous scaffolds of hydroxyapatite (HA) and polycaprolactone (PCL) using 3D printing and rapid prototyping. They designed and built three scaffold models, including a PCL sample and a modified structure of PCL and HA to enhance cell connectivity. *Shor et al.* [4] studied the percentage of porosity and calculated the mechanical properties of scaffolds made from pure PCL, as well as HA and PCL with a mass of 25 wt% HA and 60% or 70% porosity. They also examined cell survival and proliferation for osteoblast cells. *Majima et al.* [5] used a combination of sodium alginate and chitosan to create porous scaffolds, adding 5 wt% and 0.1 wt% of chitosan to sodium alginate to form polymer-based hybrids. The mechanical properties of fibers from different samples were compared, with polyglactin polymer used as a control. The number of cells remaining on the surface of the samples was also measured after 14 days. *Thuaksuban et al.* [6] built porous scaffolds for bone tissue engineering using chitosan and PCL through multilayer deposition and tensile melting, examining their physical properties and cellular response. They created 3D scaffolds of pure PCL and mass percentages of 10, 20, and 30 wt% of chitosan. The results showed that PCL with 30% chitosan showed less resistance to failure. *Gao et al* [7] utilized a fuzzy separation technique to fabricate a chitosan-gelatin-HA scaffold consisting of three components. They carefully chose ceramic and polymeric constituents that closely resembled the composition of natural bone. The density and porosity of the scaffolds were precisely regulated by manipulating the solid component and compositional variables. The researchers observed successful cellular seeding and attachment of osteoblast cells onto the porous scaffold. Notably, an increase in the ceramic phase percentage led to the enlargement of interconnected pores and facilitated the adhesion of Mesenchymal Stem Cells (MSCs).

Rodriguez et al. [8] investigated the effect of HA on porous scaffolds, fabricating a PCL-HA mixture with a 25 wt% of HA and PCL for the preparation of the porous scaffold. The significance of the current study lies in the development of a 3D porous metallic scaffold coated with chitosan containing wollastonite nanoparticles for bone tissue engineering applications [9-11]. This scaffold has demonstrated promising mechanical and biological properties, including increased elastic modulus, compressive strength, and bioactivity. Metal 3D printing is an advanced manufacturing technology that enables the use of various materials, including polymers, metal alloys, ceramics, and composites in the form of powder or wire [12-13]. Unlike traditional machining methods, 3D printing creates objects layer by layer. Selective laser melting (SLM) is a common method of 3D printing that involves using a laser as a binding agent between powder particles and layers [14-17]. In SLM, a layer of powder is placed on the manufacturing chamber, and the laser beam moves over the surface to heat specific points determined by software. This causes local binding of powder particles or their melting, and the cylinder of the manufacturing chamber is lowered one step to add another layer of powder. This process is repeated until the entire object is complete [18-20]. In the field of bone tissue engineering, the utilization of metallic

materials and 3D printing technology to create customized bone scaffolds with desirable mechanical properties has rapidly expanded. Recent research has led to the development of novel alloys with improved mechanical and biological properties for bone tissue engineering applications [19-20]. Additionally, HA/ethanolamine and nanocrystalline HA reinforced with silica-magnetite nanoparticles have been synthesized and characterized, demonstrating promising results for bone tissue engineering applications [21-22]. Coating techniques utilizing chitosan and wollastonite nanoparticles have shown potential in improving the mechanical properties of bone scaffolds. Laser welding, post-weld heat treatment, and nanoparticle coatings have been investigated for their potential in producing strong joints and enhancing the mechanical properties of metallic bone scaffolds. Several research and development in the use of metallic materials and 3D printing technology has shown great potential to advance bone tissue engineering and improve patient outcomes [20-22]. SLM is used for prototyping industrial parts and producing functional parts from various materials, primarily metals. Having knowledge of the capabilities and limitations of 3D metal printers is essential for bioengineers interested in using this technology [21-22]. Other manufacturing technique processes like Electron Beam Melting (EBM) and Ultrasonic AM (UAM) can also be used to manufacture dense metal parts. AM is a rapidly developing manufacturing technology that eliminates the need for molds, models, or fixtures, and offers greater flexibility in processing materials. AM enables the cost-effective production of single or multiple designs of a product without incurring additional costs. Since parts are made layer-by-layer, many manufacturing, assembly, and technical inspection costs are eliminated, and the final product may have no dividing lines, complications, or internal limitations. Additionally, the reduction of material waste enables the production of environmentally friendly parts. Laser-assisted AM devices are essential equipment in the automotive, jewelry, and biomedical industries for orthopedic applications. This technique enables the production of complex parts with high dimensional accuracy (up to 50 microns) using metal powder as a raw material. The porosity of the parts obtained by controlling the parameters of the machine is very low, and the mechanical properties of the parts are similar or sometimes even better than those obtained by casting. The possibility of making the final part directly from a computer file simplifies traditional manufacturing methods and frees the designer to apply more complexities in the design. Metallic 3D printers have been used to help a wide range of patients, including those with bone defects, trauma patients, and cancer patients who have defects in their bone tissue. The scaffold also showed low cytotoxicity and a good biodegradation rate, indicating its biocompatibility. The development of this scaffold has the potential to improve patient outcomes and quality of life by providing an effective and safe material for bone tissue engineering applications. This study contributes to the field of bone tissue engineering by providing a novel and effective approach to developing scaffolds that can promote bone regeneration and repair.

EXPERIMENTAL DECTION

Materials and methods

In this research, contrary to the usual methods of making polymer/ceramic composite scaffolds, the polymer components chitosan was synthesized with the wollastonite. The samples were made using three phases with the help of a 3D printer. At the beginning, the description of how to build the scaffold is described, and then the tests and analyzes performed are discussed. The wollastonite with chemical precipitation method to synthesize WS-NPs. First, we added distilled water to the wollastonite powder and stirred the mixture to obtain a homogeneous suspension. Then, we added a solution of sodium hydroxide (NaOH) dropwise to the suspension while stirring continuously until the pH reached 11. The composition was then heated and for 2 hours stirred. Then, we added a solution of ammonium carbonate ($(NH_4)_2CO_3$) dropwise to the mixture, while stirring continuously until the pH reached 8. Afterward, the mixture was subjected to stirring for an additional duration of 2 hours. Subsequently, the resulting precipitate was gathered through centrifugation and underwent multiple washes employing distilled water and ethanol. Finally, the precipitate was dried in an oven at 80°C for 6 hours to obtain WS-NPs. Fig. 1 illustrates the freeze-drying apparatus used for the chitosan coating stage, which contains wollastonite nanoparticles, on the metal scaffold. Fig. 1 shows the freeze stage used for freezing the polymeric sample onto the metal scaffold, while Image 1c shows the metal scaffold samples placed inside a falcon tube to prepare them for placement in the polymeric solution and subsequent freeze-drying (Dena Sanat Company, ISTT). To achieve homogeneity, chitosan

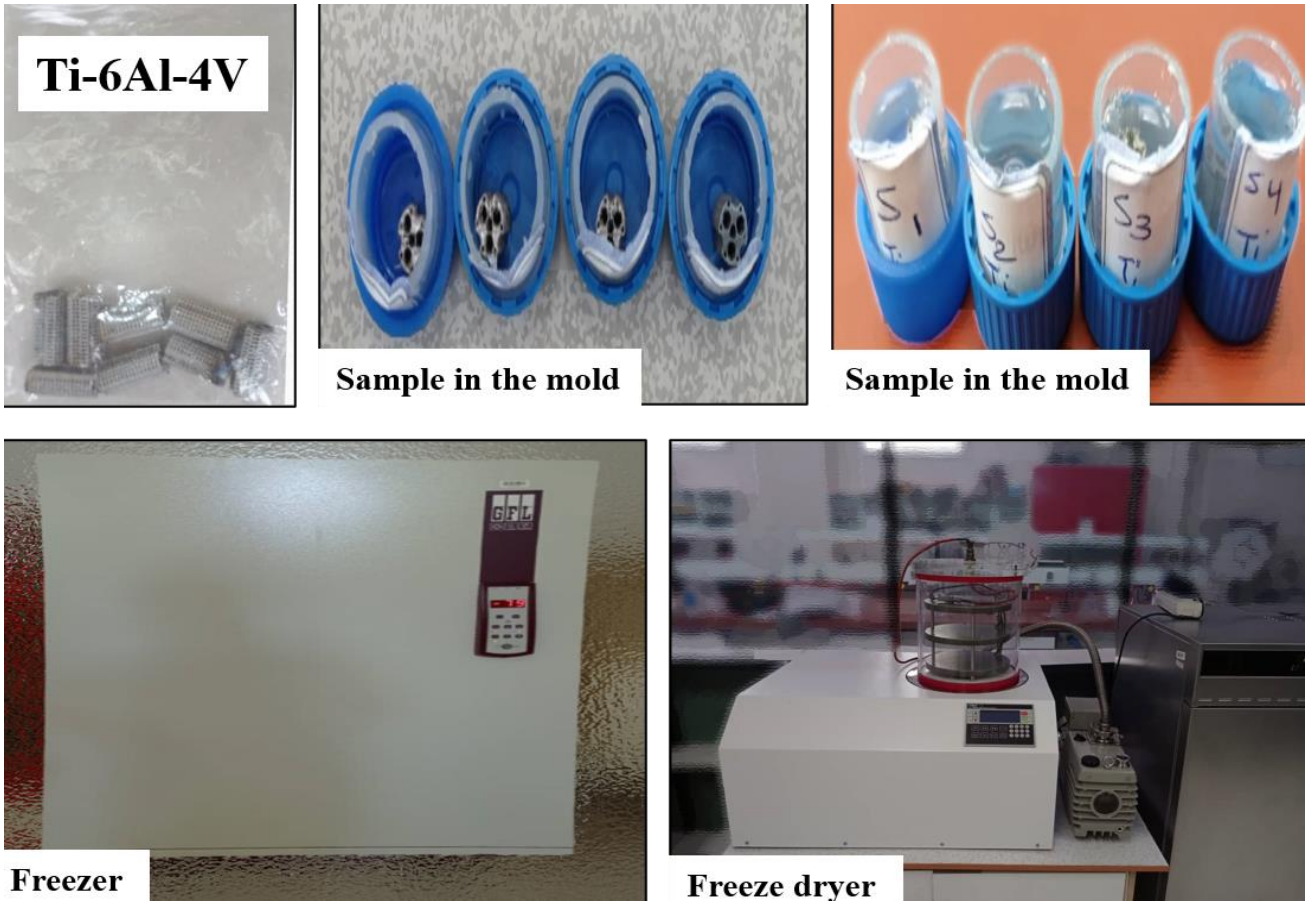

Fig. 1 : The manufacturing process of metal scaffold with chitosan-wollastonite polymer coating for use in the treatment of bone fractures.

was dissolved in the suspended solvent at a temperature of 55°C. Subsequently, a 5 mL portion of the prepared solution was introduced into a Teflon vial. The coating containing WS nanoparticles was coated on the metallic 3D-printed scaffold. The parts produced in Spadan Company Research Center using SLM and other metal 3D printing technologies can be highly practical for a range of applications. In this article, the materials used for the fabrication of porous scaffolds may be examined and then the methods used to string these materials and finally to make porous bone scaffolds. Chitosan-wollastonite coated on the matalic implant by freeze drying method. Chitosan, recognized as one of the vital natural polymers, was employed in this study. It is a linear polysaccharide composed of random units of diglucosamine and N-acetyl diglucosamine, and it is synthetically derived from chitin. For the experimental procedures, all materials, including wollastonite and chitosan with a purity exceeding 98%, were procured from Merck Germany. Wollastonite is a mineral substance with suitable physical and chemical properties for use in many biomaterial programs with various applications in the fields of medicine and dentistry. Additionally, chitosan is a polysaccharide with high antibacterial properties and tissue regeneration capabilities, and is used as one of the important materials in tissue and skin regeneration research. The preparation and use of materials with a purity of over 98% is of special importance due to the sensitivity and high importance of the materials used in biomaterial research. Merck Germany, as one of the reputable companies in the field of chemical Chitosan, owing to its solubility in aqueous solutions finds utility in the formulation of biocompatible gels, films, and fibers for medical applications. The inherent hydrophilicity and pH insensitivity of chitosan contribute to its stability. To prepare the chitosan gel as depicted in Fig. 1, an initial mixture of 8 g of chitosan and 4% acetic acid was stirred on a magnetic stirrer at a temperature of 40°C. This stirring process continued for 2 hours to ensure complete dissolution of chitosan, resulting in a highly viscous solution, as illustrated in Fig. 1. Fig. 1 depicts the thorough

dispersion of polymer and ceramic within the gel through magnetic stirring for 1 hour until a milky gel consistency is achieved. Various process parameters such as slurry viscosity, layer thickness, laser power, scanning speed, and aperture distance must be meticulously controlled. Notably, the thickness of each layer can range from 0.05 to 0.20 mm. For the production of titanium bone scaffolds, a layer thickness of 0.10 mm is chosen.

Experimental procedure

The experimental procedure commenced by dissolving chitosan (with a weight percentage of 1.6%) in a diluted solution of acetic acid (with a volume percentage of 2%) within a round-bottom flask. The flask was equipped with a continuous stirrer and a nitrogen gas inlet. The mixture was stirred for 3 hours at 60°C to ensure complete dissolution. The magnet was incorporated into the chitosan network via free radical polymerization, while bioglass nanoparticles were entrapped within the same network. The chemical formula of wollastonite, $CaSiO_3$, is a member of the mineral collection that exhibits orange to full cream luminescence. It is sparingly soluble in HCl and insoluble in water. The crystal structure is tabular with principal longitudinal directions, and it can appear white, yellow, or gray in color. Once the bio-composite coating of bioglass-wollastonite in chitosan solution was created, the next step was to apply it to the printed scaffolds. Porous scaffolds were fabricated using a 3D printer. The 3D file of the object is first saved in STL format, and then each layer is created by moving the laser and gradually building up the object. Wollastonite is classified as a silicate and is semi-transparent which the extraction method of wollastonite is shown in Relation (1).

$$CaCO_3+SiO_2 \rightarrow CaSiO_3+CO_2 \quad (1)$$

FT-IR analysis

In order to determine the chemical composition and the existing and formed bonds of the synthesized powder and composite scaffolds, infrared spectrometry and Perkin-Elmer device made in Japan were used in the range of 500-4000 cm^{-1}.

XRD analysis

To determine the constituent phases within the synthesized powder and composite scaffold, X-Ray Diffraction (XRD) analysis was conducted using an Equinox 300 instrument. The diffraction patterns were recorded within the 2θ range of 10 to 90°, employing a voltage of 40 kV and a current of 30 mA.

SEM analysis

The scaffolds were sectioned and labeled for inspection. A scanning electron microscope manufactured by Tescan in the Czech Republic, which was equipped with advanced EDS analysis capabilities, was utilized to examine the porosity of the samples and measure the diameter of the pores. Prior to analysis, the samples were coated with gold and the entire testing process took approximately 1 hour to complete. Semi-quantitative element analysis was also performed using the same instrument.

Mechanical properties

To evaluate the mechanical properties, the compressive strength tests were performed using a Hounsfield machine manufactured by the Materials Department at Isfahan University of Technology. Cylindrical samples, measuring 20 mm in length and 10 mm in diameter, were prepared and subjected to loading at a rate of 0.2 mm/min. Furthermore, the hardness of the ceramic polymer bio-nanocomposite coating was determined using a hardness measurement method on circular and cubic cavity samples. The obtained results were analyzed with a precision of SD=±3 at Isfahan University of Technology.

Porosity percentage measurement

To determine the porosity of the scaffolds, the liquid displacement method was employed. Initially, a graduated cylinder containing a specific volume of distilled water (W1) was prepared, and the dry scaffold sample was then submerged in it. The percentage of porosity was computed based on the liquid displacement method, using the Eq. (2).

$$Porosity\ (\%) = \frac{W_1 - W_3}{W_2 - W_3} \times 100 \quad (2)$$

The porosity size was determined using Image-J software. At least twenty pores from each sample were analyzed based on SEM images.

Measurement of swelling and water absorption

The swelling properties of the porous scaffolds were investigated by immersing them in both water and phosphate-buffered saline. During immersion, the scaffolds absorbed water into their porous structure, leading to an increase in their volume and weight. The degree

of swelling was determined based on the difference between the weights and volumes of the dry and swollen scaffolds. The investigation of swelling properties is important for assessing the ability of the porous scaffolds to absorb and retain fluids, which is a critical factor in various applications, such as tissue engineering.

Biological evaluation

The water absorption capacity of bone scaffolds is a vital biological characteristic that determines the performance of these composite materials. To quantitatively determine the water absorption percentage of the scaffolds, a swelling test was conducted. The scaffolds, fabricated with different proportions of polymer and ceramic phases, were cut into approximate dimensions of 1 cm by 0.5 cm. Subsequently, they were immersed in distilled water and PBS solution at a temperature of 37°C. The biological evaluation involved assessing the scaffolds in Simulated Body Fluid (SBF) and Phosphate-Buffered Saline (PBS). At specified time intervals, the scaffolds were removed from the solution until equilibrium was reached, and then weighed after removing any surface water. The percentage of water absorption was calculated using Eq. (3).

$$Swelling\ (\%) = \frac{W_2 - W_1}{W_1} \times 100 \quad (3)$$

Where W_2 and W_1 are the weight of the swollen and dry sample, respectively.

Cell culture was performed on both non-fired scaffolds and titanium-coated bone scaffolds after heat treatment at a temperature of 800°C to confirm their suitable biocompatibility. Human osteosarcoma cells (MG63) were used for cell activity analysis using the Tetrazolium Microculture Assay (MTT). The Optical Density (OD) value reflects the number of viable cells, and it was observed that the OD values increased with the duration of cell culture. Moreover, the OD values were higher for the porous scaffold compared to the green part, indicating that the porous scaffold better supports cell growth.

RESULTS AND DISCUSSION

Cozza et al. [9] synthesized HA from fish stem bone and evaluated its potential for use in tissue engineering applications through composite making with bioglass. Their results indicated that the apatitization of the natural material from fish stem bone was more successful than the industrial extraction method, and the presence of bioglass was found to be effective in promoting cell growth. Biological experiments were conducted in a SBF as well as on rats, with the results showing that the presence of bioglass improves osteooxidation. Researchers have also explored various 3D printing techniques and biomaterials for bone tissue engineering. *Lee et al*. [10] used the piezoelectric inkjet 3D printing method to make PLGA microparticles containing paclitaxel, and the drug release rate was dependent on the geometrical shape of the microparticles. *Wang et al*. [11] used SR collidon and hydroxypropyl methylcellulose to make a system containing pseudoephedrine hydrochloride with the help of 3D printing method, and the drug release rate was adjusted by changing the ratio of kollidon to Hydroxypropyl methylcellulose (HPMC). *Goyanes et al*. [12] studied the possibility of using FDM printer in making tablets containing fluorescein and investigated the effect of changing the printing parameters on the drug release curve. Despite significant progress in 3D printing technology for tissue engineering and regenerative medicine, researchers still face technical limitations in recreating complex tissues with 3D microstructures. These challenges include resolution and accuracy, material properties, biocompatibility, vascularization, and scalability. The resolution and accuracy of 3D printing can limit the production of intricate microstructures and features at a small scale. Furthermore, the mechanical properties of 3D-printed materials may not be suitable for complex tissue engineering applications, and biocompatibility issues may arise due to the use of incompatible materials. The creation of complex vascular networks remains a significant challenge in 3D tissue engineering, and producing large and intricate tissues is difficult due to limitations in the size of structures that can be printed. One promising approach to address some of these challenges is the use of bio-extrusion to create porous scaffolds. In addition to the challenges associated with 3D printing technology, the characteristics of metal powders used in AM processes, such as SLM, play a critical role in determining the properties of the final product. The chemical composition, size, morphology, and particle size distribution of the metal powders directly affect the properties of the final piece. Therefore, providing the right powder is one of the primary needs of the metal AM industry using the SLM method. Most of the world's largest producers of metal powders have defined a specific class for powders used in AM processes, which includes

Table 1: Examination of the results of the mechanical and biological properties of the manufactured samples

Sample	Elastic modulus (MPa) ± 5	Compressive strength (MPa) ± 5	Porosity (%) ± 3	Poisson ± 0.01	Density (gr/cm^3) ± 0.2
S1	410	40	45	0.31	0.85
S2	385	39	52	0.31	0.86
S3	420	43	47	0.32	1.1
S4	405	42	48	0.31	1.2
FD	22	1.4	68	0.32	1.1

the required characteristics. Technical knowledge of metal powder production is essential for ensuring the quality and consistency of the final product. This study examines the structure of 3D scaffolds made from porous titanium material using a metal printer. These porous scaffolds are coated using the freeze-drying method and are suitable for use in biomedical applications. Different porosities were achieved using a 3D printer with a polymer coating in simulations. During compression testing, the samples underwent bending, crushing, and complete disintegration, as seen in the Fig. 3. Specimen 1 experienced an identical fracture during the compression test. Deformation occurred in the longitudinal direction according to the height of the sample (the sample started to deviate from the longitudinal axis), followed by the creation of a diagonal fracture due to shear forces. After failure, the top and bottom of the specimen were completely separated.

XRD results

The microstructure of the scaffolds was examined using X-ray diffraction (XRD) analysis. Fig. 2 (a-d) illustrates the XRD patterns for chitosan, titanium, and the coated samples on the metallic nanocomposite scaffold structure. The diffraction pattern for chitosan exhibits peaks at $2\theta = 10.1°$, corresponding to the hydrated crystalline structure and amorphous structure of chitosan, respectively.

The combination of chitosan and HA has been extensively studied for its applications in tissue engineering and drug delivery. The use of XRD to analyze HA can show valuable information about how the incorporation of chitosan affects the crystal structure and properties of HA and WS. Specifically, the XRD pattern of HA may reveal a shift in the peaks of HA, suggesting a modification in its crystal structure due to the presence of chitosan. The XRD pattern shows (001) index at $2\theta = 5.4°$, which corresponds to an interlayer distance of 16.2 Å. Fig. 3 shows the mechanical properties of five samples made with specific pore sizes that were placed under compressive strength test using Hunsfield's device by applying compressive force and were deformed and sometimes broken. These deformations result in the mechanical properties of the compressive strength, elastic modulus, and Poisson's ratio as shown in Table 1. The composite layers containing wollastonite nanoparticles are gradually crushed and the strength of the samples increases gradually with the addition of reinforcing nanoparticles. The pore size of 20-50 microns is suitable for the movement of cells through the pores of the scaffold. The pore size is on average 20-40 microns.

When a load is applied to the surface of the sample, it causes the walls to collapse by involving the layers full of holes and porosity. As the compressive force increases, the compressive force decreases when the layer deforms and vice versa. The deformation process continues up to 60% deformation and eventually leads to failure. All the samples in a test group undergo static loading in the plastic deformation zone with a load value of 50-60 KN. The resulting stresses at this loading value may change up to 200-350 MPa. The maximum stress applied to the samples is up to 200 MPa with a maximum force of 50 KN. The difference between the yield stress and the ultimate stress limit is about 50 MPa, while all the samples start to crumble with about 10-20% relative compression and eventually break. Fig. 3 illustrates the maximum load bearing capacity, load application, and breaking point of 3D metal sample layers. Unsintered titanium parts for biomedical applications made using SLM are typically weak and brittle. To increase their strength, a post-baking process involving high-temperature heat treatment is applied, which is known as heat treatment. Temperatures of 700, 800, and 900 with a duration of 120 minutes have been selected for baking these biomedical titanium parts.

Based on the suitable process parameters determined through initial sample testing, a biomedical titanium bone scaffold with a hollow shell structure can be manufactured

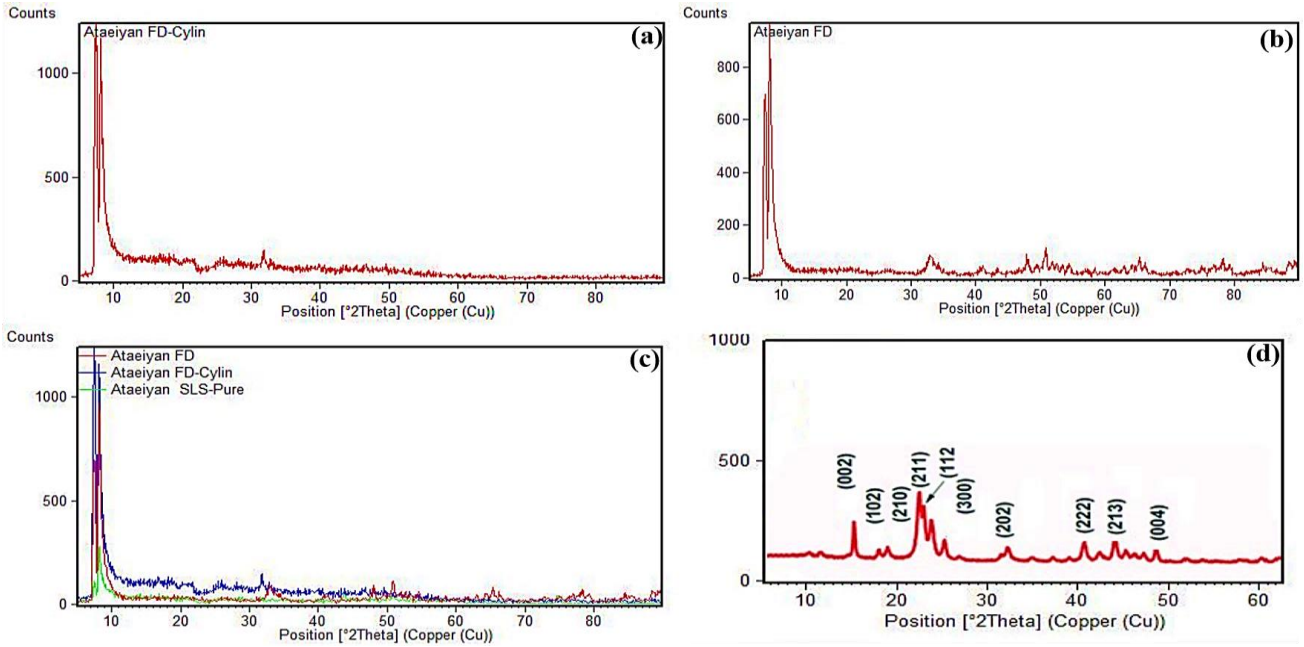

Fig. 2: XRD pattern of the a) Ti-6Al-4V, b) freeze dried sample, c) comparison of pure and coated sample, d) HA nanoparticle

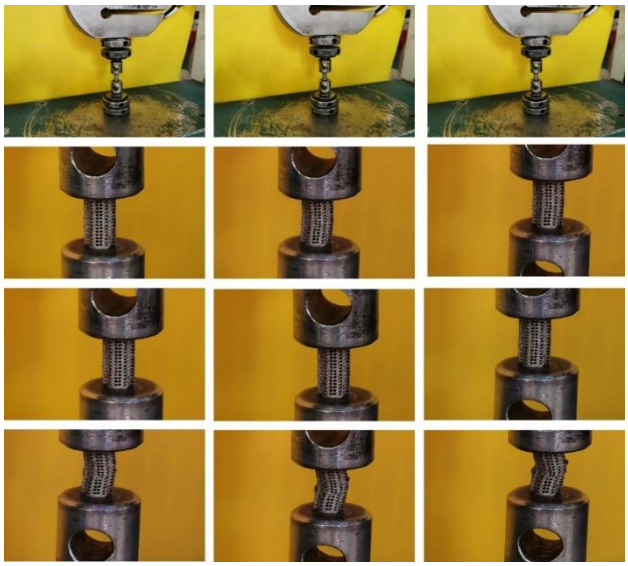

Fig. 3: Compressive strength of samples made by 3D metal printer method and freeze drying under the compressive strength

within 3 hours using the SLM process. Fig. 4 illustrates the creation of porous structures using hollow titanium nanoparticles. The manufactured samples were placed on a compression resistance platform, while mechanical stress relief due to internal stresses generated during production can cause the part to collapse. Fig. 4 shows a biomedical titanium bone scaffold produced using appropriate SLM process parameters, including a thickness of less than 100 layers, a laser power of 15 watts, a scanning speed of 100 mm per second, a hatch spacing of 0.1 mm, an energy density of 1.5 J/mm2, a beam size of 0.2 mm millimeters, and a laser frequency of 16 kHz.

Fig. 5 depicts the stress-strain curves obtained from the compressive strength testing of the samples. In contrast to conventional porous scaffolds, it exhibits a distinct deformation behavior during the compression process, where it continues to undergo elastic deformation beyond the point of highest stress. Linear elastic deformation, characterized by the elastic modulus, is observed in some of the samples. However, during the yield-stability phase, a greater linear elastic deformation, localized columnar buckling during the yield-compression phase, and ultimately complete structural yielding are observed in the samples.

After cleaning, the fabricated samples were annealed to remove the internal stresses. It is essential to remove any small parts or shavings from the sample surface to prevent premature breakage during the static pressure test that the support imposes on the sample. The results of the biological examination, including the immersion of the samples in SBF and PBS shown in Fig. 6 (a-b).

As shown in Fig. 7 (a-b), changes in the weight percentage of wollastonite nanoparticles, which contain calcium element $CaSiO_3$, affect the amount of apatitization and bone growth in the SBF. This process reaches equilibrium with long-term immersion, and in some cases, it can lead to complete dissolution of the sample.

Fig. 4: Sample preparation steps with freeze drying polymer coating with wollastonite nanoparticles

In this study, the third and fourth samples were examined using a SEM after 14 days, and significant apatite growth changes were observed. The changes in the third and fourth samples showed an increasing trend. After checking the release of ions in a SBF, it was found that the weight loss of the samples in the PBS was affected by the weight percentage of wollastonite with calcium and silica elements. During the apatitization process, the amount of silica and calcium increases the germination power, and silica has less chemical stability in phosphate-buffered saline solution, tending to absorb calcium in SBF. The samples were prepared for mechanical testing by checking their weight, measuring and scanning them using computed tomography. Each sample was printed with a resolution of 30-50 micrometers before the pressure test. Changes in the amount of calcium ions of the samples in the PBS solution indicate that the concentration of the samples is enriched after immersion in the solution, consistent with the results of weight loss. The columns parallel to the loading direction are mainly affected by tensile deformation, while inclined columns with a certain angle to the loading direction are mainly affected

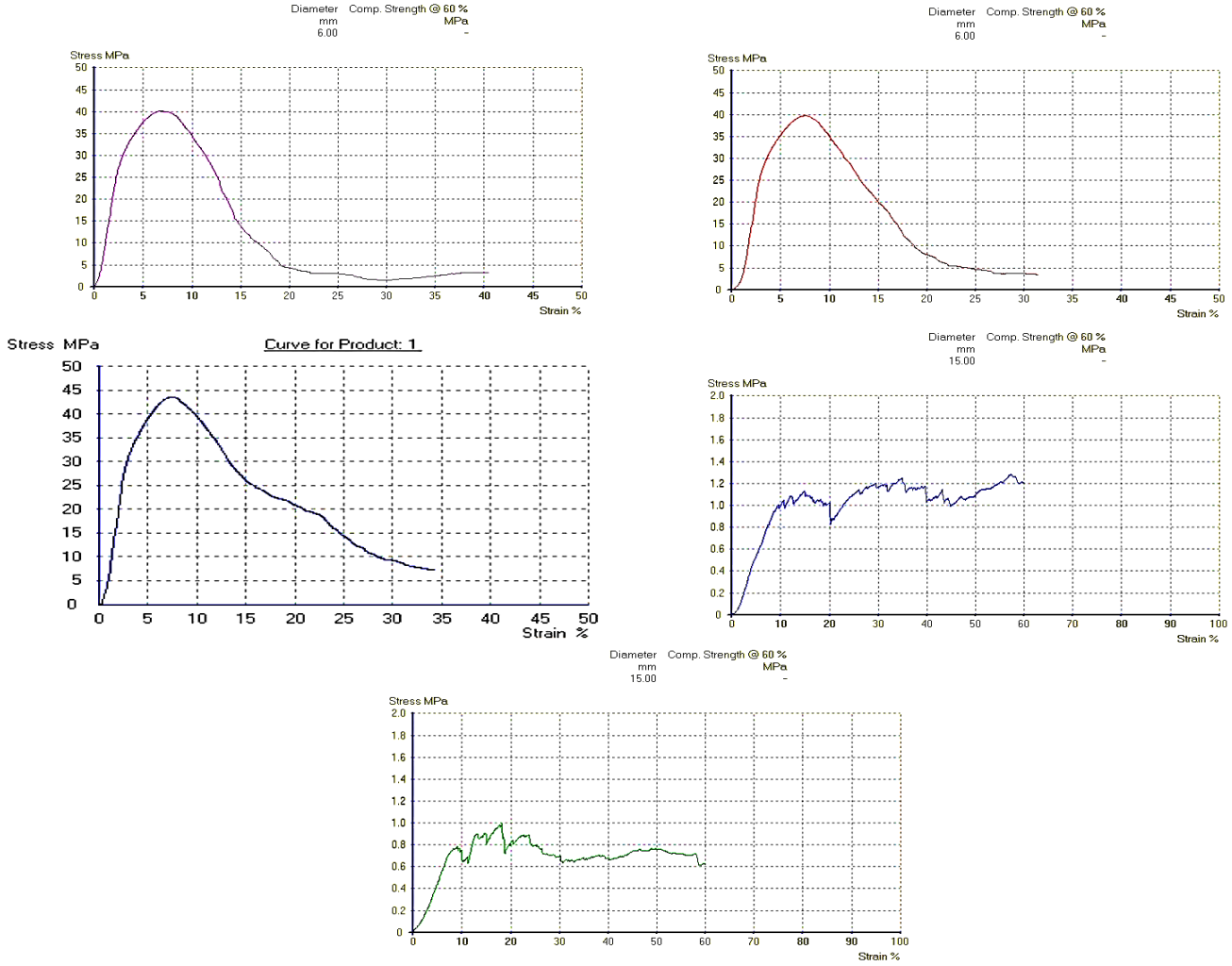

Fig. 5: Stress-strain diagram of metal 3D printed sample by SLM method for making bone scaffold under Hunsfield machine

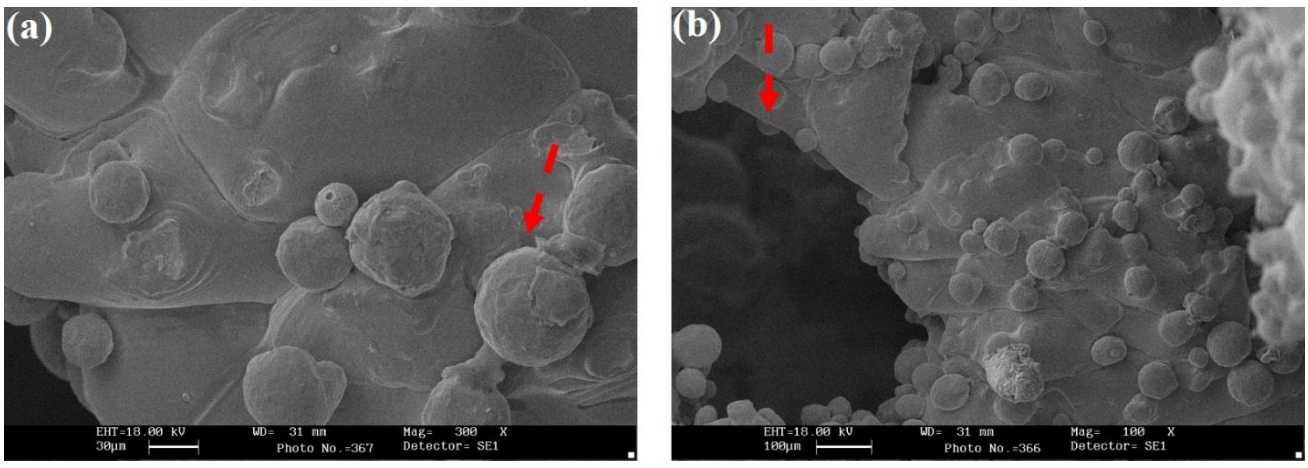

Fig. 6: SEM image of the sample containing 10 and 15 wt% of wollastonite nanoparticles in chitosan

by bending deformation. The SEM images of samples are shown in Fig. 8 (a-b). It is worth noting that the study has limitations in that it only examined the samples after 14 days, and further studies are needed to investigate long-term

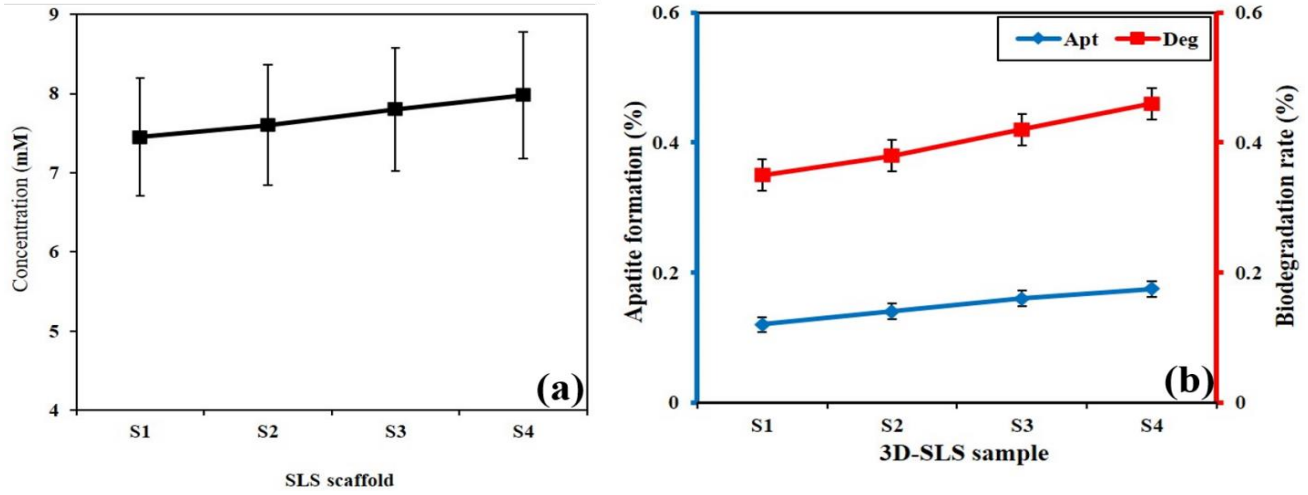

Fig. 7: Results of a) ion changes for four samples immersed in phosphate buffered saline and b) of apatite growth compared to the dissolution rate of scaffolds made by SLM method

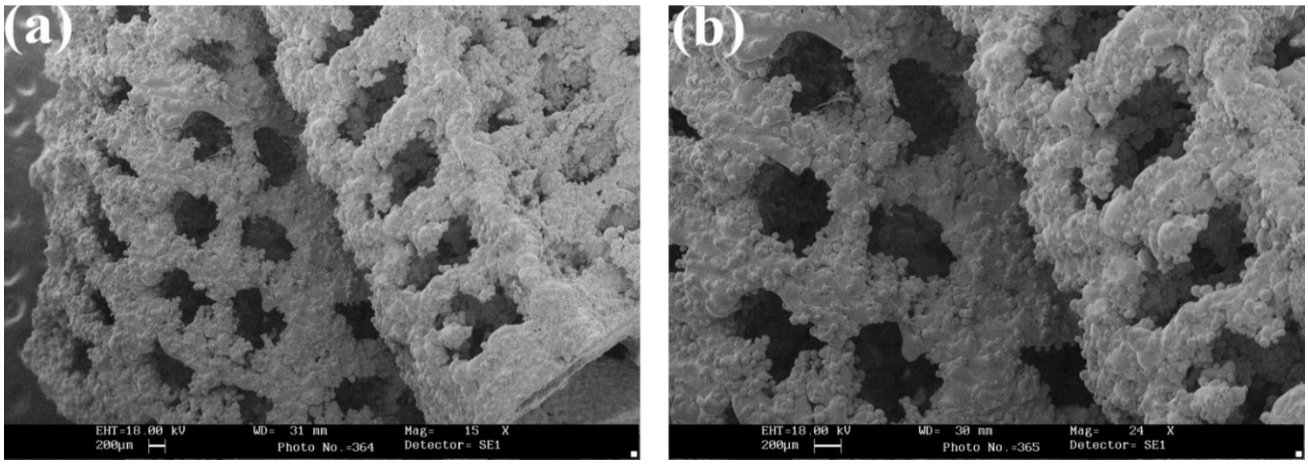

Fig. 8: SEM images of the samples soaked in the PBS for 14-21 days coated with chitosan by freeze drying technique

ossification growth changes. Finally, the study did not investigate the effect of the scaffold on cell differentiation, which could be important in determining its suitability for bone tissue engineering applications.

Fig. 8 (a-b) depicts the samples immersed in SBF after failing the compressive strength test, where the porosity of the metal scaffolds is important. The scaffolds with a porosity of about 200-300 microns shows a reduction of approximately 10-20 microns in porosity after immersion. The surface of the scaffolds printed using 3D metal printing is smooth and flat, with titanium nanoparticles joining and sintering to connect them. Fig. 8 illustrates that surface dissolution has occurred in the samples, and the remaining basic nanoparticles are in an amorphous and glassy state, indicating strong connections between the titanium nanoparticles. Fig. 8 indicates the SEM image of the surface of a porous titanium bone scaffold. Some samples were kept in non-sintered conditions in the environment, while others were subjected to heat treatment at temperatures of 700, 800, and 900°C. As the results demonstrate, the compressive strength is proportional to the post-heat treatment temperature.

Fig. 8 displays SEM images of samples fabricated using the SLM process. Microscopes and Image-J software were used to measure the pores and porosity size of each sample, and the pore size and base size distribution were relatively uniform with different specifications (Fig. 8 and Table 1). However, the examination of SEM results in Fig. 8 reveals differences between the designed size and the actual size due to powder adherence to the columns, which affects their surface quality. Sandblasting was used to clean the samples, and previous studies have shown that

vertical columns have better surface quality compared to sloped columns due to the presence of un-melted particles on the surface of the sloped columns. Each particle has a size of about 50 microns, and the addition of wollastonite nanoparticles results in stronger chemical bonding and clumping of nanoparticles, with the sample having the highest percentage by weight exhibiting the highest porosity at about 60%, observed to be 70%.

Mechanical results

To predict the mechanical properties of scaffolds fabricated using a 3D metal printer with fixed porosities, finite element analysis and simulation are performed using Abaqus software. By inputting Poisson's ratio and density of the scaffolds and having the size and shape of the pores, it is possible to predict the final stress level of the metal part and the polymer coating. The simulation results provide the maximum tolerated value of stress-strain and force-displacement diagrams for the metal scaffold. Finite Element Modelling (FEM) can reduce the cost of manufacturing mechanical samples and the error rate of results obtained from mechanical simulations. Additionally, the simulation can predict different compressive strengths for different porosities. To increase the mechanical strength of the particles, sintering is subsequently performed. During sintering, the fine-grained materials are significantly heated, with the temperature chosen below the melting point of the paste to maintain the structure of the workpiece. Examination of laboratory results for porosity and compressive strength shows that with increasing force on metal scaffolds, the porosity of the samples changes from 45 to 48%. Meanwhile, the density increases from 0.85 to 1.1 g/cm^3, with the sample having a chitosan-wollastonite coating showing a density of about 1.1 grams per cubic centimeter. Table 1 displays the mechanical properties and results of mechanical tests of metal scaffolds, which increase by adding nanoparticles to the coating. The compressive strength increases to 42 MPa as the porosity changes from 48% to 45%. Bone tissue engineering is a rapidly growing field that aims to develop new strategies for repairing or replacing damaged bone tissue [18-22]. Metallic 3D printing is a promising technology for fabricating customized bone scaffolds with desirable mechanical properties. Recent advancements in metallic materials have led to the development of new alloys with improved mechanical and biological properties for tissue engineering applications. A gradient structure Ti-55531 with ultrafine nano-sized grains was created using simulation techniques and squeeze casting, while a magnesium (Mg) alloy with exceptional room temperature formability was achieved by grain boundary segregation and activation of non-basal slip systems.

Several research studies have focused on optimizing the performance of water-lubricated bearings under transient conditions, exploring different design strategies for the application of perovskite high entropy oxides in optics [23-27]. Investigations have also been conducted on the random dynamics of rocket shell couplings with plate fasteners, examining the occurrence of welding cracks in dissimilar metal laser welds. Additionally, numerous articles have delved into the behavior of hydrogen embrittlement in hybrid welds involving stainless steel. The impact of heat input on the characteristics of the interface between bimetallic sheets in laser and cold metal transfer welding has been studied [28-32]. A novel method called attenuated velocity has been developed to measure residual stress in welding, and the effects of post-weld heat treatment on the microstructure and properties of laser-welded joints between NiTi and stainless steel have been explored [33-37]. In the field of materials science, rare earth titanates with low thermal conductivity have been designed, and the thermal protection performance of plasma-sprayed high entropy coatings has been investigated. Microstructure analysis has been conducted on compositionally complex alloys made through additive manufacturing, and the properties of bainitic steel produced through additive manufacturing have been examined [38-42]. In the field of 3D printed meta-materials, researchers have worked on regulating the compatibility of the interpenetration network interface and utilizing 3D printed thermal metamaterials to manipulate heat flow. Furthermore, insights have been provided into the bending properties of variable chain mail fabrics, and 3D honeycomb and reentrant honeycomb structures have been optimized to enhance energy absorption [43-47]. Other contributions to materials research include the study of void healing mechanisms in bearing steel, the integration of hardness and toughness in high entropy films, and the use of electromagnetic induction to improve bolt fatigue performance [48]. The process of 3D printing, also known as additive manufacturing, involves the

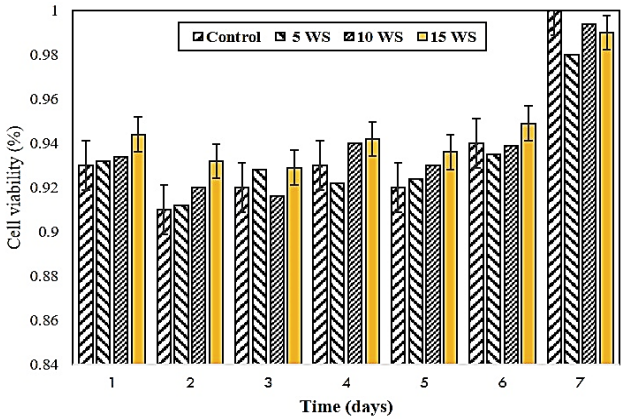

Fig. 9: The MTT assay results showed the viability of biological cells containing wollastonite. As seen in the Figure, the cell survival rate in the third and second samples is higher than the other samples, respectively.

creation of three-dimensional objects by depositing materials layer by layer based on a digital model [49-53].

Toxicity test

In this research, a bone scaffold model was designed and built using titanium metal and 3D printing technology with suitable porosity and coated with synthesized wollastonite ceramic solution. The coated scaffolds were tested to determine their mechanical properties and differences by the pressure device test. The samples were also subjected to various tests, such as the prosthesis feasibility test, bioactivity test, SEM imaging, and XRD analysis. The results demonstrated that the 3D porous metallic scaffold fabricated using SLM and coated with chitosan containing WS-NPs at varying concentrations exhibited promising mechanical and biological properties for bone tissue engineering applications. Researchers have explored various 3D printing techniques and biomaterials, such as HA, tricalcium phosphate (TCP), and biosynthetic, to improve the mechanical and biological properties of fabricated structures. The extrusion and laser powder bed fusion techniques have also garnered attention for their ability to create tissue-like structures with high precision.

Fig. 9 indicates the observation of the MTT assay for biological cells containing wollastonite. Fig. 9 shows the cell survival rate in the third and second samples is higher than the other samples, respectively. Measuring the biological activity and cell proliferation is the basis for many methods of investigating the cellular response to external factors. With this method, the cell proliferation rate can be measured, and conversely, when metabolic events lead to programmed cell death and necrosis, the decrease in cell proliferation rate can be measured. *Schappo et al*. [49] investigated the effects of adding HA to ultra-high-molecular-weight polyethylene (UHMWPE) through laser powder bed fusion for bone tissue engineering and found that this addition significantly improved both the mechanical and biological properties of the structure Computational fluid dynamics was used to study the effects of different strand orientations in 3D-printed scaffolds in perfusion bioreactors. Cuttlefish bone powder was studied for its adsorption kinetics and equilibrium of Reactive Red 198 dye [50-53]. Future studies should focus on optimizing the scaffold's properties, including its porosity, pore size, and surface roughness, and to further enhance its biological and mechanical performance. Creating 3D structures that resemble bone tissue and providing vascularization and tissue growth are major challenges in bone tissue engineering [51-53].

CONCLUSIONS

The advent of metallic 3D printing technology has enabled the production of complex medical products tailored to each patient's specific anatomical information using CAD/CAM. This approach allows for the examination of 3D bone scaffolds as models based on human bone geometry. Additionally, SEM images and XRD analyses are conducted to observe the scaffold parts' surfaces in nanometer dimensions and check the corresponding coating as well as the phases in the scaffold. The results of the mechanical and biological analyses of samples (S1-S4) indicate that their elastic modulus values range from 385 MPa to 420 MPa, with an average of 405 MPa. The compressive strength ranges from 39 MPa to 43 MPa, with an average of 42 MPa. The porosity values range from 45% to 52%, with an average of 48%. The Poisson ratios for all samples are similar, ranging from 0.31 to 0.32. The density values range from 0.85 g/cm^3 to 1.2 g/cm^3, with an average of 1.04 g/cm^3. The samples exhibit comparable properties, with slight variations in their elastic modulus, compressive strength, and porosity. In contrast, the reference material (Freeze dried) has significantly lower elastic modulus and compressive strength values but a higher porosity value than the samples, as revealed by the analyses. However, the limitations of this study include the use of in vitro testing only, and the lack of in vivo testing to confirm the scaffold's

effectiveness in promoting bone regeneration. Additionally, the study only tested one concentration of WS-NPs in the chitosan coating, and further studies are needed to optimize the concentration and assess its effects on the scaffold's properties. The study also did not investigate the effect of the scaffold on cell differentiation or gene expression, which could be important in determining its suitability for bone tissue engineering applications.

Acknowledgments

The author would like to extend their great gratitude and appreciation for the support of IAUN to this project.

Received : May 03, 2023 ; Accepted : Aug. 14, 2023

REFERENCE

[1] Wang X., Li Y., Hodgson P.D., Wen C.E., Biomimetic Modification of Porous TiNbZr Alloy Scaffold for Bone Tissue Engineering, *Tissue Engineering Part A*, **16(1):** 309-316 (2010).

[2] Hench L.L., Day D.E., Höland W., Rheinberger V.M., Glass and Medicine, *International Journal of Applied Glass Science*, **1(1):** 104-117 (2010).

[3] Park S.A., Lee S.H., Kim W.D., Fabrication of Porous Polycaprolactone/Hydroxyapatite (PCL/HA) Blend Scaffolds Using a 3D Plotting System for Bone Tissue Engineering, *Bioprocess and Biosystems Engineering*, **34(4):** 505-513 (2011).

[4] Shor L., Güçeri S., Wen X., Gandhi M., Sun W., Fabrication of Three-Dimensional Polycaprolactone / Hydroxyapatite Tissue Scaffolds and Osteoblast-Scaffold Interactions in Vitro, *Biomaterials*, **28(35):** 5291-5297 (2007).

[5] Majima T., Funakosi T., Iwasaki N., Yamane S.T., Harada K., Nonaka S., ... Nishimura, S.I., Alginate and Chitosan Polyion Complex Hybrid Fibers for Scaffolds in Ligament and Tendon Tissue Engineering, *Journal of Orthopaedic Science*, **10:** 302-307 (2005).

[6] Thuaksuban N., Nuntanaranont T., Pattanachot W., Suttapreyasri S., Cheung L.K., Biodegradable Polycaprolactone-Chitosan Three-Dimensional Scaffolds Fabricated by Melt Stretching and Multilayer Deposition for Bone Tissue Engineering: Assessment of the Physical Properties and Cellular Response, *Biomedical Materials*, **6(1):** 015009 (2011).

[7] Gao C., Deng Y., Feng P., Mao Z., Li P., Yang B., ... Peng S., Current Progress in Bioactive Ceramic Scaffolds for Bone Repair and Regeneration, *International Journal of Molecular Sciences*, **15(3):** 4714-4732 (2014).

[8] Rodriguez G., Dias J., d'Ávila M.A., Bártolo P., Influence of Hydroxyapatite on Extruded 3D Scaffolds, *Procedia Engineering*, **59:** 263-269 (2013).

[9] Cozza N., Monte F., Bonani W., Aswath P., Motta A., Migliaresi C., Bioactivity and Mineralization of Natural Hydroxyapatite from Cuttlefish Bone and Bioglass® Co-Sintered Bioceramics, *Journal of Tissue Engineering and Regenerative Medicine*, **12(2):** e1131-e1142 (2018).

[10] Lee G., Barlow J.W., Fox W.C., Aufdermorte T.B., "Biocompatibility of SLS-Formed Calcium Phosphate Implants", *1996 International Solid Freeform Fabrication Symposium* (1996).

[11] Wang C.C., Tejwani M.R., Roach W.J., Kay J.L., Yoo J., Surprenant H.L., ... & Pryor T.J., Development of Near Zero-Order Release Dosage Forms Using Three-Dimensional Printing (3-DP™) Technology, *Drug development and industrial pharmacy*, **32(3):** 367-376 (2006).

[12] Goyanes A., Martinez P.R., Buanz A., Basit A.W., Gaisford S., Effect of Geometry on Drug Release from 3D Printed Tablets, *International Journal of Pharmaceutics*, **494(2):** 657-663 (2015).

[13] Karamian E., Motamedi M.R.K., Khandan A., Soltani P., Maghsoudi S., An in Vitro Evaluation of Novel NHA/Zircon Plasma Coating on 316L Stainless Steel Dental Implant, *Progress in Natural Science: Materials International*, **24(2):** 150-156 (2014).

[14] Gligorijević B., Vilotijević M., Simulated Body Fluids Prepared with Natural Buffers and System for Active pH Regulation, *Iranian Journal of Chemistry and Chemical Engineering (IJCCE)*, **41(9):** 2918-2935 (2021).

[15] Ravi G.R., Subramanyam R.V., Calcium Hydroxide-Induced Resorption of Deciduous Teeth: A Possible Explanation, *Dental Hypotheses*, **3(3):** 90 (2012).

[16] Anttonen V., Tanner T., Kämppi A., Päkkilä J., Tjäderhane L., Patinen P., A Methodological Pilot Study on Oral Health of Young, Healthy Males, *Dental Hypotheses*, **3(3):** 106 (2012).

[17] a. Kjaer I., External Root Resorption: Different Etiologies Explained from the Composition of the Human Root-Close Periodontal Membrane, Dental Hypotheses, **4(3):** 75 (2013).
b. Narayanan, N., Thangavelu, L. Salvia Officinalis in Dentistry. *Dental Hypotheses*, **6(1):** 27 (2015).

[18] Khandan A., Karamian E., Bonakdarchian M., Mechanochemical Synthesis Evaluation of Nanocrystalline Bone-Derived Bioceramic Powder Using for Bone Tissue Engineering, *Dental Hypotheses*, **5(4):** 155 (2014).

[19] Mahjoory M., Shahgholi M., Karimipour A., investigation on the Size and Percentage Effects of Magnesium Nanoparticles on Thermophysical Properties of Reinforced Calcium Phosphate Bone Cement by Molecular Dynamic Simulation, *Heliyon*, **9:** e18835 (2023).

[20] Shojaei S., Shahgholi M., Karimipour A., The Effects of Atomic Percentage and Size of Zinc Nanoparticles, and Atomic Porosity on Thermal and Mechanical Properties of Reinforced Calcium Phosphate Cement by Molecular Dynamics Simulation, *Journal of the Mechanical Behavior of Biomedical Materials*, **141:** 105785 (2023).

[21] Shahshahani S., Shahgholi M., Karimipour A., The Thermal Performance and Mechanical Stability of Methacrylic Acid Porous Hydrogels in an Aqueous Medium at Different Initial Temperatures and Hydrogel Volume Fraction Using the Molecular Dynamics Simulation, *Journal of Molecular Liquids*, **382:** 122001 (2023).

[22] Fada R., Shahgholi M., Azimi R., Babadi N.F., Estimation of Porosity Effect on Mechanical Properties in Calcium Phosphate Cement Reinforced by Strontium Nitrate Nanoparticles: Fabrication and FEM Analysis, *Arabian Journal for Science and Engineering*, **49:** 1815-1825 (2023).

[23] Xiang G., Yang T., Guo J., Wang J., Liu B., Chen S., Optimization Transient Wear and Contact Performances of Water-Lubricated Bearings under Fluid-Solid-Thermal Coupling Condition Using Profile Modification, *Wear*, **502:** 204379 (2022).

[24] Ye S., Zhu J., Zhu S., Zhao Y., Li M., Huang Z., ... He J., Design Strategies for Perovskite-Type High-Entropy Oxides with Applications in Optics, *ACS Applied Materials & Interfaces*, **15(40):** 47475-47486 (2023).

[25] Shi X., Yang Y., Zhu X., Huang Z., Stochastic Dynamics Analysis of the Rocket Shell Coupling System with Circular Plate Fasteners Based on Spectro-Geometric Method, *Composite Structures*, **329:** 117727 (2024).

[26] Yuhua C., Yuqing M., Weiwei L., Peng H., Investigation of Welding Crack in Micro Laser Welded NiTiNb Shape Memory Alloy and Ti6Al4V Alloy Dissimilar Metals Joints, *Optics & Laser Technology*, **91:** 197-202 (2017).

[27] Fu Z.H., Yang B.J., Shan M.L., Li T., Zhu Z.Y., Ma C.P., ... Gao W., Hydrogen Embrittlement Behavior of SUS301L-MT Stainless Steel Laser-Arc Hybrid Welded Joint Localized Zones, *Corrosion Science*, **164:** 108337 (2020).

[28] Zhu Z.Y., Liu Y.L., Gou G.Q., Gao W., Chen J., Effect of Heat Input on Interfacial Characterization of the Butter Joint of Hot-Rolling CP-Ti/Q235 Bimetallic Sheets by Laser + CMT, *Scientific reports*, **11(1)**: 10020 (2021).

[29] Zhu Q., Chen J., Gou G., Chen H., Li P., Ameliorated Longitudinal Critically Refracted—Attenuation Velocity Method for Welding Residual Stress Measurement, *Journal of Materials Processing Technology*, **246**: 267-275 (2017).

[30] Chen Y., Sun S., Zhang T., Zhou X., Li S., Effects of Post-Weld Heat Treatment on the Microstructure and Mechanical Properties of Laser-Welded NiTi/304SS Joint with Ni Filler, *Materials Science and Engineering: A*, **771**: 138545 (2020).

[31] Zhu S., Zhu J., Ye S., Yang K., Li M., Wang H., He J., High-Entropy Rare Earth Titanates with Low Thermal Conductivity Designed by Lattice Distortion, *Journal of the American Ceramic Society*, **106(10):** 6279-6291 (2023).

[32] Wang K., Zhu J., Wang H., Yang K., Zhu Y., Qing Y., ... He J., Air Plasma-Sprayed High-Entropy (Y0. 2Yb0. 2Lu0. 2Eu0. 2Er0. 2) 3Al5O12 Coating with High Thermal Protection Performance, *Journal of Advanced Ceramics*, **11(10):** 1571-1582 (2022).

[33] Fang J.X., Wang J.X., Wang Y.J., He H.T., Zhang D.B., Cao Y., Microstructure Evolution and Deformation Behavior During Stretching of a Compositionally Inhomogeneous TWIP-TRIP Cantor-Like Alloy by Laser Powder Deposition, *Materials Science and Engineering: A*, **847:** 143319 (2022).

[34] Jiang Y.L., Fang J.X., Ma G.Z., Tian H.L., Zhang D.B., Cao Y., Microstructure and Properties of an As-Deposited and Post Treated High Strength Carbide-Free Bainite Steel Fabricated via Laser Powder Deposition, *Materials Science and Engineering: A*, **824:** 141791 (2021).

[35] Zhang Y., Huang Z., Wang H., Li J., Regulation of the Interface Compatibility of the 3D-Printing Interpenetration Networks Toward Reduced Structure Anisotropy and Enhanced Performances, *ACS Applied Materials & Interfaces*, **15(27):** 32984-32992 (2023).

[36] Yang S., Zhang Y., Sha Z., Huang Z., Wang H., Wang F., Li J., Deterministic Manipulation of Heat Flow *via* Three-Dimensional-Printed Thermal Meta-Materials for Multiple Protection of Critical Components, *ACS Applied Materials & Interfaces*, **14(34):** 39354-39363 (2022).

[37] Xu J., Chang L., Chen T., Ren T., Zhang Y., Cai Z., Study of the Bending Properties of Variable Stiffness Chain Mail Fabrics, *Composite Structures*, **322:** 117369 (2023).

[38] Xia B., Huang X., Chang L., Zhang R., Liao Z., Cai Z., The Arrangement Patterns Optimization of 3D Honeycomb and 3D Re-Entrant Honeycomb Structures for Energy Absorption, *Materials Today Communications*, **35:** 105996 (2023).

[39] Hua L., Liu Y., Qian D., Xie L., Wang F., Wu M., Mechanism of Void Healing in Cold Rolled Aeroengine M50 Bearing Steel under Electroshocking Treatment: A Combined Experimental and Simulation Study, *Materials Characterization*, **185:** 111736 (2022).

[40] Li Y.T., Jiang X., Wang X.T., Leng Y.X., Integration of Hardness and Toughness in (CuNiTiNbCr) Nx High Entropy Films through Nitrogen-Induced Nanocomposite Structure, *Scripta Materialia*, **238:** 115763 (2024).

[41] Zhang D., Shi D., Wang F., Qian D., Zhou Y., Fu J., ... Jiang S., Electromagnetic Shocking Induced Fatigue Improvement Via Tailoring the α-Grain Boundary in Metastable β Titanium Alloy Bolts, *Journal of Alloys and Compounds*, **966**: 171536 (2023).

[42] Jiang X.J., Bao S.J., Zhang L.W., Zhang X.Y., Jiao L.S., Qi H.B., Wang F., Effect of Zr on Microstructure and Properties of TC4 Alloy Fabricated by Laser Additive Manufacturing, *Journal of Materials Research and Technology*, **24:** 8782-8792 (2023).

[42] Zhao X., Fan B., Qiao N., Soomro R.A., Zhang R., Xu B., Stabilized $Ti_3C_2T_x$-Doped 3D Vesicle Polypyrrole Coating for Efficient Protection Toward Copper in Artificial Seawater, *Applied Surface Science*, **642:** 158639 (2024).

[43] Hu J., Yang K., Wang Q., Zhao Q.C., Jiang Y.H., Liu Y.J., Ultra-Long Life Fatigue Behavior of a High-Entropy Alloy, *International Journal of Fatigue*, **178:** 108013 (2024).

[44] Yang Z., Tang B., Qiu Y., Wu J., Wei W., Huang X., ... Wu G., Measurement of Transient Temperature Using Laser-Induced Breakdown Spectroscopy (LIBS) with the Surface Temperature Effect, *Journal of Analytical Atomic Spectrometry*, **38(10):** 1952-1961 (2023).

[45] Kuang W., Wang H., Li X., Zhang J., Zhou Q., Zhao Y., Application of the Thermodynamic Extremal Principle to Diffusion-Controlled Phase Transformations in Fe-CX Alloys: Modeling and Applications, *Acta Materialia*, **159:** 16-30 (2018).

[46] Zhao Y., Zhang B., Hou H., Chen W., Wang M., Phase-Field Simulation for the Evolution of Solid/Liquid Interface Front in Directional Solidification Process, *Journal of Materials Science & Technology*, **35(6):** 1044-1052 (2019).

[47] Yan Z., Hu Q., Jiang F., Lin S., Li R., Chen S., Mechanism and Technology Evaluation of a Novel Alternating-Arc-Based Directed Energy Deposition Method through Polarity-Switching Self-Adaptive Shunt, *Additive Manufacturing*, **67:** 103504 (2023).

[48] Meng B., Wang J., Chen M., Zhu S., Wang F., Study on the Oxidation Behavior of a Novel Thermal Barrier Coating System Using the Nanocrystalline Coating as Bonding coating on the Single-Crystal Superalloy, *Corrosion Science*, **225:** 111591 (2023).

[49] Schappo H., Salmoria G. V., Magnaudeix A., Dumur A., Renaudie E., Giry K., ... Hotza D., Laser Powder Bed Fusion of Ultra-High-Molecular-Weight Polyethylene /Hydroxyapatite Composites For Bone Tissue Engineering, *Powder Technology*, **412:** 117966 (2022).

[50] Jasemi A., Zibaseresht R., Jalali M., Nassireslami E., Hami Z., Fasihi Dastjerdi H., Fatah Hesari S., A Novel Porous Bone Scaffold Made with 3D Bioprinter Using Carboxymethyl Chitosan-Hyaluronic Acid for Knee Repair: Mechanical and Chemical Properties, *Iranian Journal of Chemistry and Chemical Engineering (IJCCE)*, **72(7):** 2142-2152 (2023).

[51] Saatchi A.R., Seddiqi H., Amoabediny G., Helder M.N., Zandieh-Doulabi B., Klein-Nulend J., Computational Fluid Dynamics in 3D-Printed Scaffolds with Different Strand-Orientation in Perfusion Bioreactors, *Iranian Journal of Chemistry and Chemical Engineering (IJCCE)*, **39(5):** 307-320 (2020).

[52] Dehvari M., Ehrampoush M.H., Ghaneian M., Jamshidi B., Tabatabaee M., Adsorption Kinetics and Equilibrium Studies of Reactive Red 198 Dye by Cuttlefish Bone Powder, *Iranian Journal of Chemistry and Chemical Engineering (IJCCE)*, **36(2):** 143-151 (2017).

[53] Wu Y., Lu Y., Zhao M., Bosiakov S., Li L., A Critical Review of Additive Manufacturing Techniques and Associated Biomaterials Used in Bone Tissue Engineering, *Polymers*, **14(10):** 2117 (2022).